Role of configurational entropy in the thermodynamics of clusters of point defects in crystalline solids

Sumeet S. Kapur, Manish Prasad, John C. Crocker, and Talid Sinno*
Department of Chemical and Biomolecular Engineering, University of Pennsylvania, 220 South 33rd Street, Philadelphia, Pennsylvania 19104, USA
(Received 28 March 2005; revised manuscript received 24 May 2005; published 20 July 2005)

The internal configurational entropy of point defect clusters in crystalline silicon is studied in detail by analyzing their potential energy landscapes. Both on-lattice and off-lattice calculation approaches are employed to demonstrate the importance of off-lattice configurational states that arise due to a large number of inherent structures (local minima) in the energy landscape generated by the interatomic potential function. The resulting cluster configurational entropy of formation is shown to exhibit behavior that is qualitatively similar to that observed in supercooled liquids and amorphous solids and substantially alters the thermodynamic properties of point defect clusters in crystals at high temperature. This behavior is shown to be independent of interatomic potential and cluster type, and suggests that defects in crystals at high temperature should be generally described by a quasicontinuous collection of nondegenerate states rather than as a single ground state structure. The modified thermodynamic properties of vacancy clusters at high temperature are found to explain a long-standing discrepancy between simulation predictions and experimental measurements of vacancy aggregation dynamics in silicon.

DOI: 10.1103/PhysRevB.72.014119 PACS number(s): 61.72.Bb, 61.72.Qq

I. INTRODUCTION

Clustering of point defects and impurity atoms in crystalline materials is a ubiquitous phenomenon that affects a host of material properties. The growth and processing of crystalline semiconductor materials such as silicon, silicon alloys, and gallium arsenide, for example, is almost completely dominated by rules aimed at minimizing the number of defects such as point defect clusters,[1,2] dislocations,[3] and stacking faults.[4] Similarly, in metal alloy systems, the microscopic distribution of the component species can often critically affect the mechanical and chemical properties of the alloy.[5] Given the importance of nucleation and growth of clusters in materials processing, there has been much effort aimed at the development of simulation tools for predicting the relationship between processing conditions and the resultant properties (i.e., cluster size distribution) of a material.[6] Most such tools require as input the thermodynamic properties of the various species in a system as a function of temperature, cluster size and composition.

The properties of small atomic clusters, however, are extremely difficult to measure experimentally. As a result, there has been substantial effort aimed at the structural and thermodynamic characterization of clusters using atomistic simulations; for example self-interstitial and vacancy clusters in silicon have been studied extensively with empirical potentials,[7,8] tight-binding potentials,[9,10] and density functional theory.[11,12] Much of the atomistic simulation work on cluster characterization has focused exclusively on minimum energy configurations in order to make a thermodynamic and structural description tractable. On the other hand, processing in both metallic and semiconductor systems is often accomplished at elevated temperature where entropy can be important, particularly vibrational and configurational entropy.

In this paper we compute the total free energy of point defect clusters in crystalline silicon at finite temperature based on an analysis of the potential energy landscapes[13,14] created by the clusters. The configurational entropy of small clusters is found to be surprisingly large and leads to significant corrections to the free energies of defect clusters. We focus primarily on the study of vacancy clusters in silicon using the environment-dependent interatomic potential[15,16] (EDIP) but show that our results and conclusions are applicable to other types of clusters and (classical) potential systems and therefore could have broad implications for the thermodynamic analysis of defects in solids. Two different computational frameworks for calculating cluster free energies are used. The first is based on Monte Carlo simulations in a discrete, on-lattice representation of the system, while in the second continuous-space molecular dynamics simulations are employed.

The remainder of the paper is organized as follows. In the next section, the general thermodynamic framework for computing the free energy (including the configurational entropy) of clusters is outlined. An on-lattice model for vacancy cluster thermodynamics is presented in Sec. III, followed by an off-lattice treatment in Sec. IV. Extensions to self-interstitial clusters and other interatomic potentials are discussed in Sec. V and conclusions are presented in Sec. VI.

II. THERMODYNAMICS OF AGGREGATION

Single species aggregation is generally described by a series of coupled, reversible interactions between clusters of different sizes

$$X_i + X_j \underset{F(i,j)}{\overset{K(i,j)}{\leftrightarrow}} X_{i+j}, \tag{1}$$

where X_i is the concentration of clusters of size i, and $K(i,j)$ and $F(i,j)$ are the coalescence and fragmentation kernels,

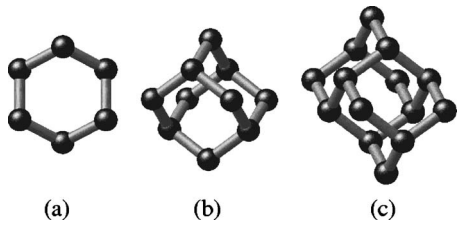

FIG. 1. Hexagonal ring clusters (HRCs) containing (a) 6, (b) 10, and (c) 14 vacancies.

respectively. Coalescence and fragmentation rates depend on both kinetic and thermodynamic factors, i.e.,

$$K(i,j) = A_{ij}(D_i + D_j)\exp\left(-\frac{G^B_{i+j\rightarrow(i+j)}}{k_B T}\right), \tag{2}$$

where A_{ij} is a size and morphology dependent geometric factor, D_i is the mobility of cluster i, and $G^B_{i+j\rightarrow(i+j)}$ is the free energy barrier associated with the coalescence of clusters i and j. The latter is usually expressed as[17]

$$G^B_{i+j\rightarrow(i+j)} = \Delta G_{i+j} - \Delta G_i - \Delta G_j - kT\ln\left(\frac{\Omega_2}{\Omega_1}\right), \tag{3}$$

where ΔG_i is the formation free energy of a cluster of size i. The last term in Eq. (3) represents the change in the translational entropy of the system.[18] As defined here, the translational entropy only includes configuration space associated with the cluster centers of mass.

The free energy of formation of an atomic cluster in a crystal contains several thermodynamic contributions,

$$\Delta G = \langle \Delta E \rangle - T\langle \Delta S_{vib} \rangle - TS_{conf}, \tag{4}$$

where ΔE is the formation enthalpy, ΔS_{vib} is the vibrational entropy of formation,[19–21] and S_{conf} is the cluster configurational entropy. The $\langle\,\rangle$ indicate averaging over all the individual configurations that the cluster can possess.

The cluster configurational entropy is the number of distinguishable configurations that a particular cluster can possess *per lattice site*. Note that the cluster configurational entropy is fully excluded from the translational entropy as defined above and therefore the total number of ways of distributing clusters in a lattice is given by $\Omega_{tot} = \Omega_{trans}\Pi_i \Omega_i^{conf}$, where the product index is over all clusters in the system. This configurational entropy is often neglected because it is difficult to estimate analytically except for very simple structures.

A. Vacancy clusters in silicon

Most continuum models for aggregation that require cluster thermodynamics as input assume that the ground state morphology is a good representation. For vacancies in silicon the ground state morphology is the so-called hexagonal ring cluster (HRC) configuration, which is formed by maximizing the number of complete hexagonal vacancy rings.[9,22] Examples of HRC structures are shown in Fig. 1. The HRC morphology naturally evolves into regular octahedral structures with (111)-oriented surfaces at larger sizes,[23] and in this case the cluster configurational entropy can be assumed to be negligible.

While the HRC morphology is a reasonable representation of large clusters at low temperatures, much of semiconductor processing takes place at high temperatures. Our previous atomistic simulations[18] employing the classical EDIP potential demonstrate that vacancy clusters at elevated temperature spend a majority of the time in spatially extended configurations that are much higher in energy than the ground state. The fact that vacancy clusters can assume these extended configurations arises from the large vacancy-vacancy interaction distance, which has been shown to extend up to about 7.8 Å, corresponding to the 4th neighbor shell along the (110) direction (4NN-110), or the 8th-nearest neighbor shell overall.[18]

B. Cluster formation thermodynamics from the potential energy landscape

In the following discussion we employ the concept of inherent structures (IS) in a potential energy landscape (PEL). Inherent structures, as introduced by Stillinger and Weber,[24] are local minimum configurations in the 3N-dimensional potential energy surface,[13] defined by the coordinates of an N-atom system. A *basin* is defined as the set of points in phase space that map to the same IS when the system is quenched using local energy minimization. The basin construct is useful because it partitions the total phase space of the system into a set of non-overlapping local minima connected by saddle points.

The concepts of inherent structures and potential energy landscapes have existed for a long time[13] and have recently been successfully applied to the study of configurational entropy in supercooled liquids and glasses.[25,26] On the other hand, the IS/PEL framework has not yet been applied to the study of defect formation properties in crystals because small defect clusters in crystals are not associated with substantial configurational entropy. In the following discussion, we briefly outline the IS/PEL thermodynamic framework as applied to the formation properties of defect clusters in crystals. Note that all simulations in this paper are performed at zero pressure and no distinction is made between the Helmholtz and Gibbs free energies.

In general, the free energy of a system in the canonical ensemble is given by

$$G = -k_B T \ln Z, \tag{5}$$

where Z is the canonical partition function:

$$Z = \frac{1}{N!}\frac{1}{\Lambda^{3N}}\int \exp(-V(\mathbf{r}^N)/k_B T)d\mathbf{r}^N. \tag{6}$$

In Eq. (6), $\Lambda = (h^2/2\pi m k_B T)^{1/2}$ is the thermal de Broglie wavelength that arises from integration of the kinetic portion of the partition function, and $V(\mathbf{r}^N)$ is the potential energy of the system, which depends only on the 3N-dimensional position vector, $\mathbf{r}^N$. Applying the IS picture introduced above, the partition function can be rewritten as

$$Z = \frac{1}{\Lambda^{3N}} \sum_{\alpha} \exp(-\beta V_{\alpha}) \int_{R_{\alpha}} \exp(-\beta \Delta V_{\alpha}(\mathbf{r}^N)) d\mathbf{r}^N, \quad (7)$$

where $\beta = 1/k_B T$, V_{α} is the minimum potential energy in basin α, $\Delta V_{\alpha}(\mathbf{r}^N)$ is the potential energy relative to the minimum for a particular configuration in basin α, and R_{α} is the set of configurational phase space points contained in basin α. Further assuming that basins are uniquely characterized by their minimum energy, V_{α}, Eq. (7) can be rewritten as[24,26]

$$Z = \frac{1}{\Lambda^{3N}} \int g(V_{\alpha}) \exp(-\beta V_{\alpha}) \exp(-\beta G_{vib}(\beta, V_{\alpha})) dV_{\alpha}, \quad (8)$$

where $g(V_{\alpha})$ is the density-of-states function (DOS) for the distribution of basin energy minima. The temperature-dependent quantity $G_{vib}(\beta, V_{\alpha})$ represents the (vibrational) free energy of a basin with minimum energy V_{α}, i.e., $G_{vib}(\beta, V_{\alpha}) \equiv -TS_{vib}(V_{\alpha})$, and $S_{vib}(V_{\alpha}) \equiv k_B \ln N_{vib}$, where N_{vib} is the number of vibrational states in a basin. Therefore, Eq. (8) can be rewritten as

$$Z = \frac{1}{\Lambda^{3N}} \int G(V_{\alpha}) \exp(-\beta V_{\alpha}) dV_{\alpha}. \quad (9)$$

The DOS function $G(V_{\alpha})$ represents the distribution of *both* configurational and vibrational states, i.e., $G(V_{\alpha}) = N_{vib} g(V_{\alpha})$. Assuming that in a perfect crystal system only a single configurational state exists, the free energy is then given by

$$\begin{aligned} G_p &= -k_B T \ln[N_{vib}^p / \Lambda^{3N} \exp(-\beta V_p)] \\ &= 3Nk_B T \ln \Lambda + V_p - TS_{vib}^p. \end{aligned} \quad (10)$$

For a system containing a feature such as a vacancy cluster, the density-of-states function also must account for multiple configurational states:

$$G_d = -k_B T \ln \int \tilde{G}(V_{\alpha}) N_{vib}^{ref} N_{conf}^{ref} / \Lambda^{3N} \exp(-\beta V_{\alpha}) dV_{\alpha}, \quad (11)$$

where the superscript "ref" indicates a reference configuration for each cluster (to be defined) and the "tilde" notation indicates that the density of states is normalized so that it is unity at the reference state, i.e., $\tilde{G}(V_{\alpha}) = G(V_{\alpha}) / G(V_{\alpha}^{ref})$. Employing the definition of vibrational entropy given above, Eq. (11) can be rewritten as

$$G_d = -TS_{vib}^{ref} - k_B T \ln \int \tilde{G}(V_{\alpha}) N_{conf}^{ref} / \Lambda^{3N} \exp(-\beta V_{\alpha}) dV_{\alpha}. \quad (12)$$

Note that in Eqs. (11) and (12), N represents the number of atoms in the defected system. For the specific case of vacancy clusters, the formation free energy of a cluster containing N_V vacancies is

$$\Delta G \equiv G_d - G_p \left(\frac{N_h - N_V}{N_h} \right), \quad (13)$$

where N_h is the number of atoms in the perfect crystal reference system. Combining Eqs. (10), (12), and (13), the formation free energy for a vacancy cluster is given by

$$\Delta G = -T\Delta S_{vib}^{ref} - k_B T \ln \int \tilde{G}(\Delta E) N_{conf}^{ref} \exp(-\beta \Delta E) d(\Delta E), \quad (14)$$

where ΔE is the formation enthalpy of a cluster and is approximately independent of temperature. A similar expression can be written for any type of cluster and Eq. (14) is the fundamental starting point for our free energy calculations. Finally, the probability distribution function $p(\Delta E) \equiv G(\Delta E) \exp(-\beta \Delta E)$ can be directly sampled with equilibrium molecular dynamics. For discrete, on-lattice systems, $g(\Delta E)$ can be computed directly as shown in the following section.

III. ON-LATTICE CALCULATIONS OF CLUSTER FREE ENERGY

The IS/PEL framework generally has been applied to continuous space systems. Here, we extend its application to a discrete on-lattice model for vacancy clusters. On-lattice vacancy clusters are defined as clusters that are formed by removing a set of atoms from a perfect crystal lattice, followed by lattice relaxation with molecular statics. The PEL in discrete space is similar to one in continuous space at zero temperature and consists of a collection of infinitely narrow basins separated by inaccessible phase space. Sampling of this space must be accomplished by moves designed to hop directly from basin to basin. Equation (14) from the previous section is directly applicable to this situation except that the vibrational entropy contribution associated with each discrete configuration must be computed separately.

The recently developed Wang-Landau Monte Carlo[27] (WLMC) method was used to investigate the thermodynamics of on-lattice vacancy clusters and generate a density-of-states function for each cluster. The WLMC approach was used because of the large energy differences between the various cluster configurations, which would lead to severe sampling bottlenecks in a standard Metropolis Monte Carlo simulation.

First, an n-vacancy cluster was generated by removing n atoms from a perfect crystal lattice. The configurational density-of-states function for the formation energy, $g(\Delta E)$, and the visit histogram, $h(\Delta E)$, were initialized to unity and zero, respectively. Both $g(\Delta E)$ and $h(\Delta E)$ were discretized using 0.1 eV energy bins. A cluster was defined as connected based on the Stillinger criterion[28] and an interaction range of up to 7.8 Å was assumed. The vacancy positions were identified by comparison of the quenched lattice to a reference perfect lattice at the same density. The positions of reference atoms that were unmatched by corresponding atoms in the actual lattice were assigned to vacancies.

Monte Carlo (MC) moves were performed by moving a single randomly selected atom (vacancy) to another location

picked at random from all sites that were within the interaction distance to at least one of the other atoms (vacancies). Note that this is a biased move basis because not all the possible destination sites are considered in the selection. We discuss the bias correction below. In addition, moves that led to fragmented cluster configurations (based on the Stillinger definition) were rejected without further evaluation. For the remaining cases, the formation energy of the cluster configuration was calculated by relaxing the lattice statically at constant volume using a conjugate gradient energy minimization scheme[29] and then applying Eq. (13).

The WLMC acceptance/rejection criterion for accepting a move from formation energy level ΔE_1 to ΔE_2 is given by

$$p(\Delta E_1 \rightarrow \Delta E_2) = \min\left[\frac{g(\Delta E_1)}{g(\Delta E_2)}, 1\right]. \tag{15}$$

Each time a formation energy level ΔE is visited the current density-of-states value is multiplied by a factor $f>1$ so that $g(\Delta E)=g(\Delta E)f$. The multiplicative factor f is initially set to a value of exp(1) in our simulations, i.e., $f_1=2.718282$. Concurrently, the visit histogram is updated by adding one to the value at that energy level so that $h(\Delta E)=h(\Delta E)+1$. The simulation proceeds until a minimum flatness criterion is achieved in the function $h(\Delta E)$, which is taken here to be 85%. Once this criterion is achieved, the value of f is reduced according to the schedule $f_{i+1}=\sqrt{f_i}$, where, i represents the number of simulation "stages," and $h(\Delta E)$ is reset to zero. Our simulations were executed until $f_1=1.000001$.

The WLMC simulation only provides the density-of-states function up to an arbitrary multiplicative constant. In order to compute an absolute free energy from Eq. (14) it is necessary to specify the absolute number of states in at least a single energy interval and thereby anchor the $g(\Delta E)$ function. The reference state used in all the ensuing calculations in this paper is the HRC configuration because it is relatively easy to isolate and possesses relatively few configurations, which can be counted directly.

A special note should be made regarding the simulation cell sizes used throughout this work. In principle, there is an extremely wide variation in the cluster sizes possible for a given number of vacancies, ranging from a compact sphere, all the way to a linear chain at maximum extension between the vacancies (8NN). It is not computationally practical to set the system size based on the theoretical maximum sized cluster because this would require extremely large simulation cells. However, because of the very low probability that such clusters will be encountered; a much smaller cell can usually be used. In all cases, the system size was chosen so that no size effects were apparent in the results. For 8NN-connected clusters we used cells ranging from 512 atoms for 2 vacancies to 5832 atoms for 35 vacancies.

A. Validation of the WLMC approach

The WLMC algorithm was validated by comparison to a direct counting approach. Obviously, the direct counting approach is limited because of the relatively small number of configurations that can be stored in memory. A comparison between the direct counting and WLMC predictions for the DOS of a nearest-neighbor-connected 6-vacancy (6V) cluster (i.e., the Stillinger interaction distance is set to the 1st-nearest neighbor distance) is shown in Fig. 2. Both approaches show a three state DOS function where the lowest energy state is the HRC configuration (6-atom ring) that has two orientations per lattice site. The other two states are substantially higher in energy but possess about 3×10^2 equivalent orientations.

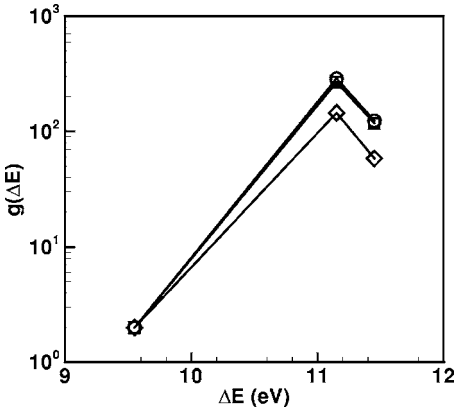

FIG. 2. DOS for a 1st-nearest neighbor connected 6-vacancy cluster calculated using (a) WLMC (diamonds) and (b) direct counting (circles). Also shown are the results from a corrected-bias WLMC (squares).

A systematic discrepancy is apparent between the results of the direct counting and WLMC calculations, which does not disappear as the visit histogram flatness criterion is increased. The discrepancy arises because of the way the destination sites are selected. In general, all empty sites must be considered in the selection of a destination site for a hop. However, the vast majority of moves performed in this way would lead to infeasible structures that do not contribute to the *cluster* density of states, and the simulation would be prohibitively expensive due to the high rejection rate. The constraint that cluster connectivity be preserved during sampling implies that the number of transitions possible from any given configuration is not uniform. For example, a linear cluster with all monomers arranged at maximum interaction distance can only accommodate moves through its end atoms. On the other hand, a more spherical cluster has many more redundant connections and therefore many more possible "outbound" transitions.

A bias-corrected WLMC algorithm was generated by modifying the acceptance probability of a transition [Eq. (15)] so that

$$p(\Delta E_1 \rightarrow \Delta E_2) = \frac{C_1}{C_{\max}} \min\left[\frac{g(\Delta E_1)}{g(\Delta E_2)}, 1\right], \tag{16}$$

where C_1 is the number of possible outbound transitions from the state "1" and $C_{\max}$ is the maximum number of outbound transitions for any state in the system.

The number of possible transitions is computed by looping over each atom in the cluster and finding the number of locations that it can be moved to while preserving the cluster connectivity. The maximum is estimated at the beginning of

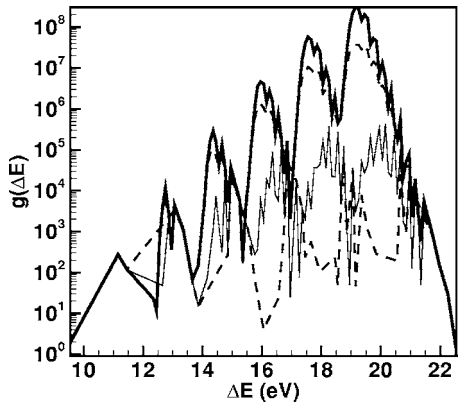

FIG. 3. DOS for 6V cluster as a function of vacancy-vacancy interaction distance. Lower dashed: 2NN; thin solid: 3NN; upper dashed: 6NN; thick solid: 8NN.

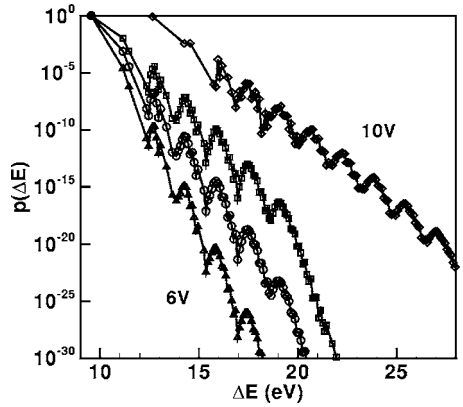

FIG. 4. Probability distribution functions for the 6V cluster at (a) 1600 K (squares), (b) 1300 K (circles), and (c) 1000 K (triangles) and the 10V cluster (diamonds) at 1600 K.

the simulation—note that overestimation of this number does not affect the results but only reduces the efficiency of the simulation by leading to more rejections. The bias-corrected WLMC simulation results for the 6V-1NN cluster are also shown in Fig. 2 and show excellent agreement with the direct counting results.

B. Dependence of the DOS on interaction distance

The effect of increasing the interaction range between vacancies on the DOS function for the 6V cluster is shown in Fig. 3. The DOS function is seen to rise dramatically with increasing interaction range and for the 8th-nearest neighbor case has a value of 3×10^8 at 19.5 eV, which is 10 eV higher than the ground state. Obviously, it is not practical to use the direct counting approach for this case. Also note that as the interaction distance increases the form of the DOS function becomes more easily discernable as an exponentially increasing function.

The periodic peaks are due to the sudden increase in states as each additional particle is moved away from the cluster core. Also note that as the interaction distance increases, the DOS exponent also increases—the significance of this feature will be discussed in more detail in Sec. IV. Finally, the decay in the DOS at the end is due to the fact that fewer states are available for stretched configurations.

C. Probability distribution functions for on-lattice vacancy clusters

The probability distribution function (PDF) for the on-lattice system is given by

$$p(\Delta E) = G(\Delta E)\exp(-\beta\Delta E) = g(\Delta E)\exp(-\beta\Delta E)\exp(S_{vib}(\Delta E)/k). \quad (17)$$

Note that the vibrational entropy dependence has to incorporated explicitly because the different vibrational states associated with each configuration are not sampled with the on-lattice WLMC simulations. Calculations of the vibrational entropy of formation as a function of cluster configuration and energy are discussed further in Sec. IV B. The distribution function in Eq. (17) can be interpreted as the probability distribution of states obtained from a molecular dynamics simulation that is restricted to only sample on-lattice cluster configurations.

The probability distribution, $p(\Delta E)$, for the 6V cluster at 1000 K, 1300 K, and 1600 K is shown in Fig. 4. All distributions are arbitrarily anchored so that the probability distribution function is unity at the ground state. While the relative importance of higher energy states increases with increasing temperature, the ground state (corresponding to the HRC configuration) is dominant even at 1600 K, which is close to the melting temperature of silicon. The 2nd-lowest energy state ($\sim$11 eV) is about 100 times less probable at 1600 K and 1×10^5 times less probable at 1000 K. States with higher energies are progressively less represented. In other words, even the combination of both the vibrational and on-lattice configurational entropy near the melting temperature is still not sufficient to compensate for the higher energy of any state relative to the HRC configuration.

Also shown in Fig. 4 is the probability distribution for the 10V cluster at 1600 K, which leads to a similar picture, although the decay of the probability distribution function is slower than that for the 6V case, reflecting the faster exponential increase in the DOS function for the 10V cluster. Simulations for clusters up to size 30V fail to show any appreciable impact from non-ground state configurations at all temperatures up to 1600 K. Based on these results the total free energy of formation for EDIP vacancy clusters is adequately represented by the free energy of the HRC configuration for all cluster sizes and at all temperatures. In other words, while the on-lattice potential energy landscape does contain a large number of states, the density is not high enough to appreciably contribute to the free energy.

IV. OFF-LATTICE CALCULATIONS OF CLUSTER FREE ENERGY

Extended EDIP molecular dynamics simulations at 1600 K (and to a lesser extent at lower temperatures) show that vacancy clusters spend a majority of time in states that are of much higher energy than the HRC configuration. This

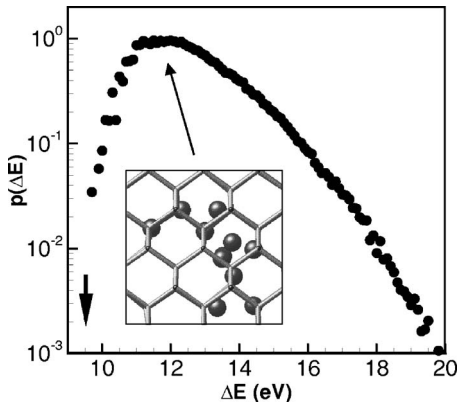

FIG. 5. Probability distribution function for a 6-vacancy cluster at 1600 K obtained directly from MD. Inset: Spheres represent atoms displaced by more than 10% of a bond length.

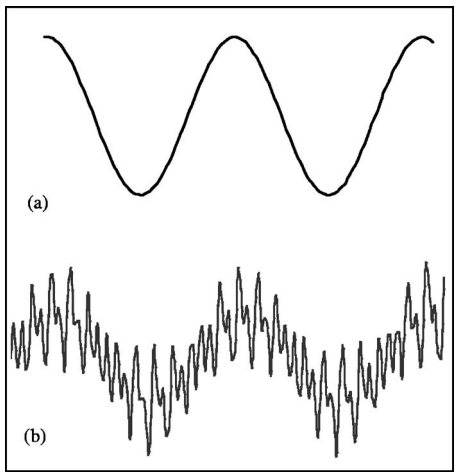

FIG. 6. Potential energy surface experienced by a single hopping atom in a crystal (a) without lattice rearrangements and (b) with lattice rearrangements.

is particularly significant given the predicted high binding energy of the HRC configuration for the 6V vacancy cluster in silicon. Very long NVT-ensemble (zero pressure) MD trajectories of a 1000-lattice site cell containing a 6V cluster were periodically quenched (approximately every 100–200 time steps) to the local energy minimum and the formation energies collected into bins as in the on-lattice WLMC calculation described in the previous section.

The resulting PDF is shown in Fig. 5 and exhibits several fundamental differences relative to the on-lattice MC case. Most importantly, the dominant states are now located at approximately 11.8 eV while the HRC ground state is *never* observed during the simulation which was run for about 8×10^7 time steps or about 50 ns of real time. The distribution also is now much shallower than for the discrete case, which implies that a larger number of configurations contribute to the average thermodynamic properties. Finally, many of the unoccupied bins in the on-lattice case (e.g., states between 9.5 eV and 11.0 eV) are now populated and the distribution appears to be almost continuous. In fact, the energy spacing between states is less than 0.01 eV in some regions of probability distribution function.

An example (quenched) configuration of the simulation lattice in the neighborhood of the 6V cluster is shown in the inset of Fig. 5. The configuration possesses formation energy in the region of the peak of the distribution (11.8 eV). Several neighboring atoms are significantly displaced from their lattice positions to the extent that it is no longer possible to definitively assign vacancies to particular lattice sites. Other configurations found in the MD simulation show similar off-lattice character and spatial extension, with the higher energy structures becoming increasingly disordered and extended. The increased stability of higher energy structures arises from the tremendous number of possible configurations if substantial off-lattice rearrangements are allowed. Although off-lattice relaxations were permitted in the WLMC calculations during the energy minimizations, these were only sufficient to sample the *local* minimum in the potential energy surface near an on-lattice configuration.

The fact that each configuration sampled using the above procedure corresponds to a well-defined local minimum in the potential energy surface was confirmed by repeated coordinate perturbation followed by reminimization. Even states that were separated by less than 0.01 eV (the tolerance of our CG minimizations) were reproducibly isolated by energy minimization following coordinate perturbation. Of course, this robustness was observed only if the perturbations did not exceed a certain critical value (about 2–3 % of a bond length)—perturbation magnitudes above this value led to relaxations into different local minima. In general, these local minima possessed substantially different energies (up to $\sim$1 eV) from the original value. Conversely, states with adjacent formation energies were generally found to correspond to substantially different atomic configurations.

The results above indicate that the potential energy surface contains a large enough density of local minima to substantially alter the thermodynamics of vacancy clusters. This view is schematically represented in Fig. 6, which contrasts the conventional view (a) of a smooth potential surface experienced by a hopping point defect in a crystal and the present picture (b). The situation in (b) is not unlike the potential energy surface expected in an amorphous solid or supercooled liquid, but here is localized to the vicinity of the defect. Note that these states are introduced into the system by the presence of the point defect and would not otherwise exist in the perfect lattice. In other words they are a property of the defect and therefore modify its thermodynamic properties. The defect clusters therefore act as strong sources of amorphization within the lattice, an idea that has been qualitatively suggested in the literature for many years[30] but has not yet been quantitatively analyzed.

We note here that multiple off-lattice configurations for defect clusters have been found and analyzed in recent tight-binding MD calculations, specifically for small self-interstitial clusters in silicon.[31] However, the enormous number of distinct configurations located in the present work leads to a fundamentally different physical picture in which the cluster thermodynamics are qualitatively altered as will be shown in the subsequent sections. In Refs. 31 and 32, only a few structures were isolated which would not lead to a significant configurational entropy contribution, but do

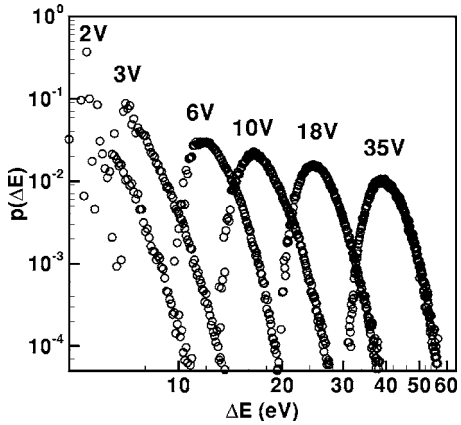

FIG. 7. Probability distribution function for vacancy clusters at 1600 K obtained directly from MD.

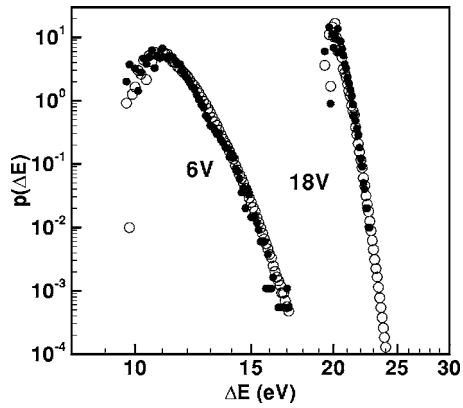

FIG. 8. Overlap between probability distributions sampled at two different temperatures for the 6V and 18V clusters. Solid symbols: low T; open symbols: high T. All data shown is scaled to the lower temperature (1400 K for 6 V; 1050 K for 18 V).

have important effects on the diffusion path as shown in Ref. 32.

A. Absolute probability distributions and density-of-states functions

The PDFs for several other vacancy clusters containing 2–35 vacancies were also generated using direct MD; examples are shown in Fig. 7. All distributions have been arbitrarily normalized to unit area. As the cluster size increases, the range of energies sampled by the cluster also increases and, for the 35-vacancy cluster, the difference between the energy at the distribution peak and the HRC structure is about 10 eV or 75 k_BT. Except for dimers and trimers, the distributions are observed to be almost continuous across the entire range of sampled formation energies, with well-defined peaks at intermediate values. For clusters containing more than 4 vacancies, the HRC configuration was never observed at 1600 K, while in the dimer and trimer cases the clusters were observed to revisit the HRC configuration multiple times.

The PDFs in Fig. 7 are known only to within a multiplicative constant, which must be determined before they can be used to compute absolute free energies. As in the discrete case, anchoring of a PDF requires knowing the state count in at least one energy bin within the distribution, and in the on-lattice simulations the HRC configuration was used for this purpose. While the HRC configuration is still a natural anchor for the off-lattice distributions, it is more difficult to utilize it because the 1600 K MD simulations do not visit this state as discussed above.

This difficulty was resolved using a second MD simulation at lower temperature in which the HRC structure was sampled adequately while maintaining sufficient overlap with the 1600 K distribution. This approach is conceptually similar to umbrella sampling[33] in which distributions across different energy subintervals are overlapped to create a complete one. The optimal temperature for the second simulation was determined by balancing the requirement that the HRC configuration be sampled adequately with the need to maximize the overall transition rates to produce a distribution with sufficient statistics in a reasonable amount of CPU time. In fact, the low temperature "anchor" simulations accounted for most the overall computational effort in this study. The high temperature simulations are still required because they sample the cluster configurations much more rapidly and provide better overall statistics over most of the energy range.

Examples of the two-temperature approach are shown in Fig. 8 for the 6V and 18V clusters. In the 6V case, the low temperature simulation was performed at 1400 K while for the 18V cluster a temperature of 1050 K was used. Note that for both the 6V and 18V clusters, the distributions are plotted at the low temperature; i.e., the 6V distributions are shown at 1400 K and the 18V distributions at 1050 K. While almost full overlap between the low and high temperature distributions could be achieved in the 6V case, the large temperature difference between the two simulations used for the 18V case implied that only a relatively small part of the distributions overlapped ($\sim$3–4 eV in the formation energy range) and could be used for anchoring the 1600 K data.

The corresponding absolute density-of-states functions (obtained by sampling at 1600 K) for the various cluster sizes are shown in Fig. 9. The solid black circle symbols are the (directly counted) density of states for the HRC configurations. Also shown for the 6V and 18V clusters are DOS functions obtained from the low-temperature simulations, which are seen to overlap extremely well with the corresponding high-temperature data. Each of the DOS functions rises exponentially after an initial deviation, and appears to be unbounded. This exponential growth in the DOS functions is not inconsistent with the concept of a thermodynamically stable cluster because the distributions in Fig. 7 are bounded. In other words, even though DOS functions grow exponentially, the magnitude of the Boltzmann factor exponent is larger. Physically, the unbounded DOS functions point to the fact that each cluster can spawn an infinite number of higher energy states—in fact, the states near the tail end of the DOS functions in Fig. 7 possess energies that are higher than a completely dissociated cluster, even though they represent valid Stillinger clusters. These configurations correspond to the formation of additional defect structures such as Frenkel pairs (interstitial-vacancy pairs)[34] and other

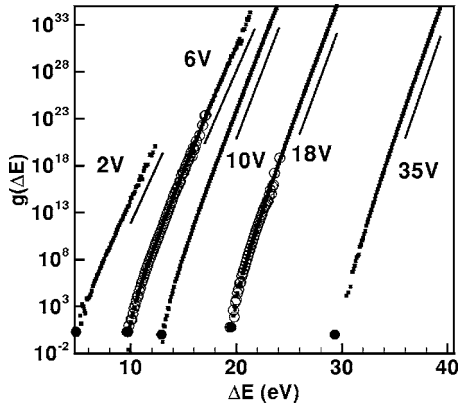

FIG. 9. Absolute density-of-states functions. Small squares: data derived from sampling at 1600 K; solid circles: directly counted HRC degeneracy; large open circles: DOS sampled at 1400 K (6V) and 1050 K (18V); thin solid lines: exponential fits.

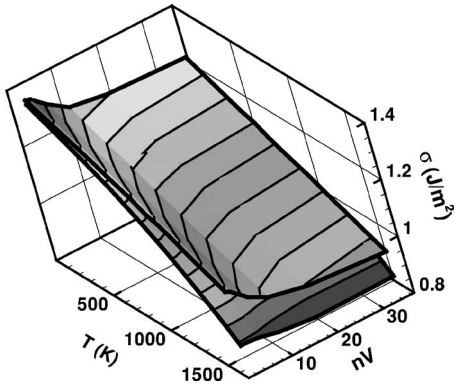

FIG. 11. Temperature and size dependence of the total effective surface free energy (σ) of vacancy clusters predicted using the EDIP potential. Lower surface: current results including configurational entropy; upper surface: HRC calculations with vibrational entropy only.

types of disordered states, and suggest a mechanism for amorphization and even crystal melting.

A plot of the DOS exponents as a function of cluster size is shown in Fig. 10 in which the exponents have been expressed as effective temperatures, i.e., $G(\Delta E) \sim \exp(\beta_{eff}\Delta E)$, where $\beta_{eff} \equiv 1/kT_{eff}$ is the fitted exponent for a given DOS. For effective temperatures above the crystal melting temperature ($\sim$1520 K), the probability distribution, $p(\Delta E)=G(\Delta E)\exp(-\beta\Delta E)$ is bounded and the crystal is stable. As shown in Fig. 10, the effective temperature appears to approach this limit as a power law in the cluster size over the range studied, although larger cluster sizes would be required to completely determine the limiting behavior. In other words, the additional states introduced by clusters provide a path for crystal melting to occur, and larger clusters produce a higher state density.

B. Total cluster free energy calculations

The distribution functions shown in Figs. 7 and 9 were used to compute free energies of formation for each of the clusters, which are a critical ingredient in continuum simulations of aggregation. The formation free energies were computed as a function of cluster size and temperature using Eq. (14). Details of the vibrational entropy calculation for the HRC configuration are given below in Sec. IV C.

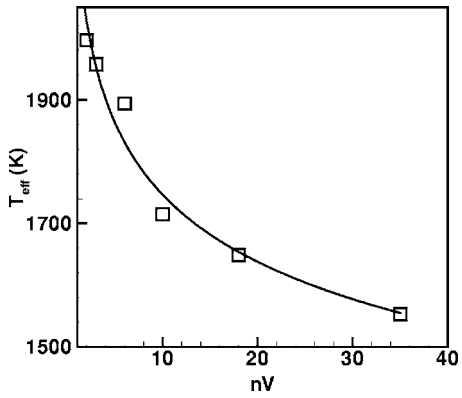

FIG. 10. DOS exponent dependence on cluster size. Line is a power-law fit.

The temperature and size dependence of $\Delta G(n,T)$ is shown explicitly in Fig. 11 (lower plane) by defining an effective surface free energy as $\sigma=\Delta G(n,T)/\alpha n^{2/3}$, where $\alpha = 2.224$ for a sphere.[35] Also shown is the surface free energy obtained using conventional ground state calculations in which the enthalpy and vibrational entropy of formation for the HRC are computed as functions of temperature (upper plane). Several observations can be made. First, the surface energies computed using both approaches converge at low temperature where the configurational entropy is negligible. The agreement at low temperature provides a good consistency check because the present results are extrapolated from high temperature using the density-of-states function. At high temperatures, a substantial deviation between the predicted surface energies is apparent because the surface energy predicted by including the configurational entropy decreases more strongly with temperature than the HRC curve. The deviation is greatest for small clusters because the relative effect of configurational entropy is greatest for these sizes.

Interestingly, at high temperatures the effective surface energy predicted in the present work is approximately constant over the size interval $2<n<35$, implying that the free energy of formation scales as $n^{2/3}$ for all cluster sizes considered. In addition, based on previous analyses, the 35-vacancy cluster is fully representative of the continuum limit because it is the smallest structure that can assume a perfect (111) faceted octahedral shape.[18] As a result, the present calculations indicate that the surface free energy scales as $n^{2/3}$ for *all* sizes at elevated temperatures. At lower temperatures, however, the smallest clusters clearly possess higher effective surface free energy and deviate from the $n^{2/3}$ scaling law (for both sets of calculations). The observed deviation for small clusters arises because at low temperatures the effect of configurational entropy is negligible and the atomistic (discrete) nature of the clusters leads to a higher effective surface free energy as observed in previous thermodynamic

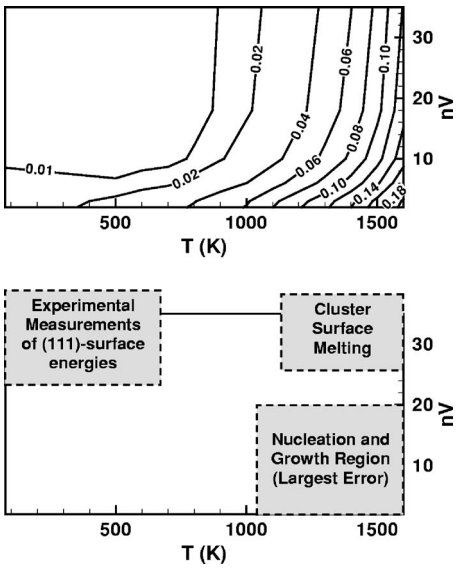

FIG. 12. (a) Difference ratio, $(\sigma_{HRC}-\sigma_{FULL})/\sigma_{FULL}$, between current ($\sigma_{FULL}$) and HRC ($\sigma_{HRC}$) surface free energies as a function of EDIP temperature and vacancy cluster size; (b) relevant physical phenomena as a function of temperature and vacancy cluster size.

analyses.[18] By contrast, in the HRC calculations, the increase in effective surface free energy for small clusters is present at all temperatures because the atomic discreteness of the HRC structure is preserved (by construction).

A more direct comparison between the present calculations and the HRC results is shown in Fig. 12(a). The contour lines represent the difference between the ground state HRC and total surface free energy calculations from this work, defined as $(\sigma_{HRC}-\sigma_{FULL})/\sigma_{FULL}$. At low temperatures the configurational entropy is negligible for all but the smallest cluster sizes and a ground state analysis is appropriate, i.e., the error is less than 2%. At temperatures above about 1100 K, the deviation between the two approaches increases especially for small clusters: the difference for $2<n<6$ at 1600 K is larger than 20%. In addition, a persistent error of about 12% appears for larger sizes at 1600 K. As mentioned earlier, because the 35-vacancy cluster is a perfect octahedron [comprised entirely of (111) surfaces] this difference is expected to apply to all subsequent sizes.

The "phase" plot in Fig. 12(b) provides a comprehensive view of the effect of configurational entropy in size and temperature space. The maximum discrepancy for small clusters at high temperature is critically important because small clusters are the primary species present during the early, high temperature stages of nucleation and growth of aggregates during silicon crystal growth (see below). Thus a ground state analysis of the thermodynamics of these species is incorrect at the temperatures relevant to nucleation.

At temperatures above about 1300 K the difference between the ground state analysis and the present one persists at all sizes as mentioned above. The reason for this discrepancy is due to surface melting. Larger vacancy clusters are well approximated by internal (111) surfaces, which melt at a temperature substantially below the bulk melting temperature of 1685 K. The (111) surface melting temperature predicted by the EDIP is approximately 1200–1300 K, and above this temperature, a vacancy cluster at any size will exhibit some surface melting because of the extremely high density of states associated with off-lattice disorder created by this process. Surface melting at temperatures below the bulk melting temperature has important implications during the processing of the silicon wafers because it provides a pathway for cluster dissolution during wafer thermal annealing.

1. Connections to experimental data

The heretofore-neglected contribution of the configurational entropy to vacancy cluster free energy is obviously important in the context of modeling microvoid formation during Czochralski (CZ) crystal growth. During this process, vacancy aggregation is initiated at high temperature because of vacancy supersaturation that results from crystal cooling. Continuum models for void formation have shown unequivocally that low (i.e., $\sim$0.75–0.85 J/m^2) values of σ are necessary to predict the correct nucleation onset temperature [approx. 1350–1400 K (Ref. 36)]. On the other hand, it has been difficult to reconcile this range of values for the cluster surface free energy with experimental measurements of the (111) surface energy at 77 K, which are clustered around 1.25J/m^2.[37–39] As mentioned earlier, the (111) surface is widely considered as a good basis for estimating the free energy of experimentally observed octahedral voids, which consist almost entirely of (111)-oriented surfaces.[40] Our prediction for the effective surface free energy of the 35V cluster, which is entirely comprised of (111) surfaces, decreases from about 1.24 J/m^2 at 77 K to 0.82 J/m^2 at 1600 K.

Based on the present results, it is now possible to consolidate both values with a single result. The large clusters that are experimentally observed in commercial single-crystal silicon after cooling are unaffected by configurational entropy, and are well described by the (111) surface energy model (upper left region in Fig. 12). However, early during the nucleation process, small clusters at high temperature are spatially extended due to a combination of configurational and vibrational entropy and are therefore characterized by a much smaller effective surface free energy (lower right region in Fig. 12). A single experimental data point available in the literature at the melting temperature of silicon (1685 K) (Ref. 41) provides a lowered (111) surface free energy (0.89 J/m^2) and further supports the validity of the present picture.

It should be noted that the excellent quantitative agreement between EDIP predictions and the experimental measurements in Refs. 37–39 and 41 is likely to be partially fortuitous. EDIP underpredicts the melting temperature of silicon by about 10%, which may lead to comparable uncertainty in the predicted temperature dependence. In fact, 1600 K is slightly above the thermodynamic melting temperature (but substantially below the mechanical melting point) of the EDIP potential, which is about 1530–1560 K. Therefore, properties computed with EDIP between 1550 K and 1600 K roughly correspond to those of real silicon at its experimental melting temperature.

The interest in Si(111) surface free energies has been fueled by the need for predictive continuum scale simulators to calculate the size distribution and density of voids in commercial Czochralski-grown silicon crystals. The impact of vacancy cluster configurational entropy on such models was investigated in detail by applying the physics obtained in this work to an existing void dynamics simulator.[2] We find that the simulator is now able to simultaneously predict, for the first time, correct void sizes, densities, and nucleation temperatures for a very wide range of crystal growth operating conditions. Most importantly, this was achieved with no parameter fits that have been the hallmark of previous studies. These findings are beyond the scope of the current paper and are presented in detail in Ref. 42.

C. Explicit calculation of the cluster configurational entropy

While the configurational entropy is intrinsically taken into account in Eq. (14), it is not possible to directly compute it from the total free energy. Rearranging Eq. (4), the configurational entropy for a cluster is given by

$$TS_{conf} = \langle \Delta E \rangle - T\langle \Delta S_{vib} \rangle - \Delta G, \tag{18}$$

which requires that the configurationally averaged formation energy and vibrational entropy be calculated. The former is directly obtained from the probability distribution functions. As mentioned in Sec. II, the vibrational entropy of a given configuration was determined using the quasiharmonic approximation[19] following static relaxation at constant volume. The QHA was performed at 1000 K for all configurations, although it was determined that the QHA computed vibrational entropy did not depend on temperature over a large range.

The configurationally averaged vibrational entropy of formation was computed by repeated QHA analysis for a wide range of configurations (and formation energies) at each cluster size. The resulting formation entropies for each cluster size were then fitted to linear functions of formation energy and the configurational average computed as

$$\langle \Delta S_{vib} \rangle = \sum \Delta S^i_{vib}(\Delta E_i) \times p'(\Delta E_i), \tag{19}$$

where $p'(\Delta E_i)$ is the normalized probability distribution function for the formation energies and $\Delta S^i_{vib}(\Delta E_i)$ represents the functional dependence of the formation vibrational entropy on the formation energy. The temperature dependence of the configurational entropy contribution to the free energy is shown in Fig. 13 for several cluster sizes. As the cluster size increases, the temperature dependence becomes stronger. Note that at low temperatures, the total configurational entropy for the smaller clusters is larger than that of the larger clusters, but the trend is reversed at high temperature because of the stronger temperature dependence. In fact, in the case of the 35V clusters the entropic contribution to the free energy is negligible below about 1000 K.

These trends can be explained by the fact that although larger clusters require more thermal energy to substantially fragment because they are more tightly bonded they have a much larger configurational space to explore once sufficient energy is provided. Also shown in Fig. 13 is the expected limiting behavior for large clusters. The onset of the sudden explosion in the configurational entropy corresponds to the melting of the internal (111) surfaces. This picture further supports the hypothesis presented in Sec. IV B.

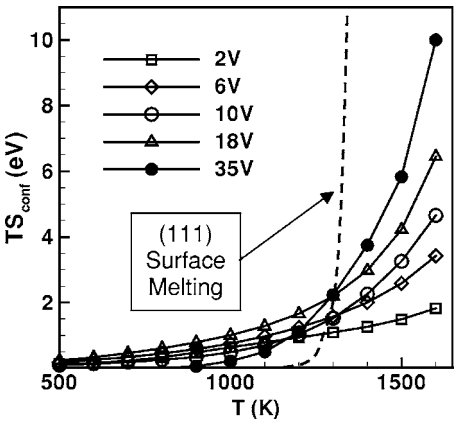

FIG. 13. Configurational entropy contribution to the free energy of formation as a function of temperature for various cluster sizes. Dashed line: limiting behavior for (111) surface melting.

D. The single vacancy

The thermodynamics of the single silicon vacancy have been studied numerous times using a wide variety of computational methods. Here we demonstrate that the configurational entropy picture presented in the previous sections can even influence the properties of single point defects. This is a surprising result because the single vacancy thermodynamic properties are generally assumed to be well described by a single ground state. The single-vacancy probability distribution and density-of-states functions for the formation energy are shown in Fig. 14. As in the cluster case, a distribution of formation energies are found, ranging from the ground state value of 3.25 eV found in earlier work with the EDIP potential,[18] to values as high as 8 eV which correspond to the additional formation of an interstitial-vacancy complex. While the probability distribution is strongly peaked at the ground state configuration, the total contribution of the first few higher energy states is about 20% of the ground state

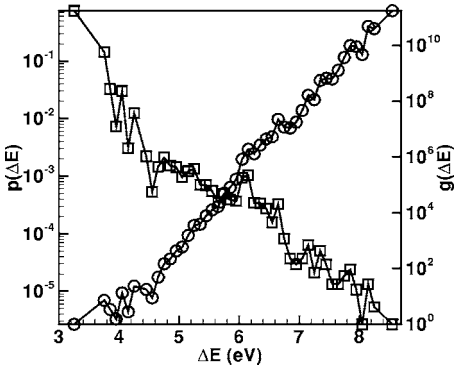

FIG. 14. DOS (circles) and PDF (squares) at 1600 K for the single vacancy.

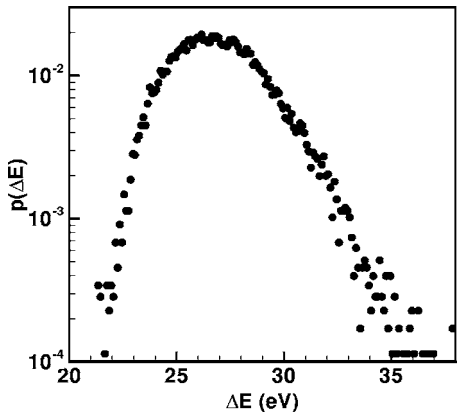

FIG. 15. Probability distribution function for the 10-interstitial cluster in EDIP silicon.

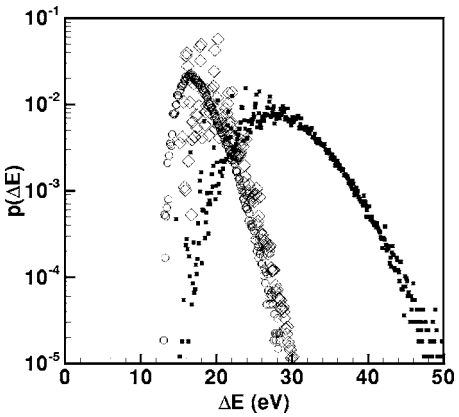

FIG. 16. Probability distribution function for the 10V cluster. (a) Solid squares: Tersoff potential at 2700 K; (b) open diamonds: Tersoff potential at 2650 K; (c) open circles: EDIP potential at 1600 K.

free energy. This corresponds to a temperature dependent shift in the predicted equilibrium concentration of about 100% at 1600 K. Given that the contributing excited states are at only slightly higher energy relative to the ground state, this effect persists as the temperature is lowered.

These results suggest that many defects at high temperature should be characterized thermodynamically as a collection of nondegenerate states, rather than a single ground-state structure. The dense PEL induced by larger structures leads to substantial amorphization, but even single point defects introduce enough states to cause deviation from ground state thermodynamics. In fact, the present approach even can be applied to the perfect crystal, which can be considered to be the ground state configuration in a sequence of progressively higher energy states. This was examined by performing extended MD simulations of a perfect crystal with periodic minimizations. The DOS for the perfect crystal (not shown) indicates that at least one excited state (2.5 eV above the ground state) is accessible by direct MD at 1600 K. Inspection of the lattice corresponding to this configuration shows that the local minimum corresponds closely to the so-called fourfold coordinated defect recently identified with DFT calculations,[43,44] which was also found to have formation energy of 2.5 eV. This correspondence serves to highlight the generality of the physical picture presented here as well as ability of the EDIP potential to accurately identify and model bulk defects in silicon.

V. EXTENSION TO OTHER POTENTIAL MODELS

The applicability of our results to other systems was investigated further by considering a self-interstitial cluster using the EDIP potential and vacancy clusters using the Tersoff potential for silicon.[45,46]

A. Self-interstitial clusters in EDIP silicon

The probability distribution function for the 10-interstitial cluster at 1600 K is shown in Fig. 15. Clearly, the same general trends observed for the vacancy cluster cases also are seen here, namely that the ground state (~21 eV) is not relevant for describing the thermodynamic properties of the cluster. The peak in the distribution is located at 26 eV. In principle, the calculation of formation free energies from this distribution is identical to the vacancy case. However, an additional difficulty arises in the anchoring of the distribution because, unlike the vacancy case, the ground state for self-interstitial clusters is morphologically complicated and cannot be counted directly. The general problem of distribution anchoring for complex defect structures is not trivial and further work is needed to extend the present approach to such species.

B. Vacancy clusters in Tersoff silicon

A final test of the generality of our results was performed using the Tersoff potential for silicon. The probability distribution function for the 10V cluster at 2700 K in Tersoff silicon is shown in Fig. 16 (solid squares). This temperature corresponds very roughly to 1600 K within the EDIP framework as determined by matching single vacancy diffusion coefficients. A similar picture is obtained in which the cluster is characterized by a distribution of states that are significantly higher in energy than the ground state configuration.

Also shown in Fig. 16 (open symbols) is the EDIP probability distribution function at 1600 K and the Tersoff distribution function rescaled to a temperature of 2650 K. Note how the small temperature shift leads to a large change in the probability distribution function and that the Tersoff distribution function at 2650 K is now very close to the EDIP curve, confirming the reproducibility of the physics across interatomic potentials. On the other hand, it is difficult to resolve differences in vacancy diffusion coefficients at 2650 K and 2700 K because of the scatter in the measurements. In other words, temperature matching using the single vacancy diffusion coefficient essentially gives the same result as matching the probability distribution curves and in fact demonstrates the universality of the present results with respect to choice of interatomic potentials.

VI. CONCLUSIONS

We have demonstrated that configurational entropy is a qualitatively important contribution to the thermodynamic

properties of atomic clusters in crystalline solids, particularly at elevated temperature. The magnitude of this entropic source is strongly underestimated if a lattice-based approach is used because of the presence of an unexpectedly large number of off-lattice local minima in the potential energy surface. The present calculations suggest that any lattice defect should be interpreted as a dense collection of nondegenerate states, in which the ground state may or may not be relevant at high temperature, which is a fundamentally different view than the traditional approach of basing finite temperature property calculations on the minimum energy structure.

The overall picture presented here for the crystalline silicon system is shown to be independent of the empirical potential or the type of defect cluster, and suggests that the computational approach and results presented here should be generally applicable to other solid-state systems. Our results also have implications for multiscale modeling approaches in which molecular dynamics simulations are used to compute properties for coarser models such as on-lattice kinetic Monte Carlo. The loss of degrees of freedom in the latter implies that the configurational entropy associated with the off-lattice states is lost and will substantially alter the thermodynamic properties of the system. The question of how to effectively account for this lost entropy will be the subject of future work.

ACKNOWLEDGMENTS

We gratefully acknowledge financial support from the National Science Foundation (CTS01-34418).

*Email address: talid@seas.upenn.edu

[1] H. Föll, U. Gösele, and B. O. Kolbesen, J. Cryst. Growth **52**, 907 (1981).
[2] T. Sinno and R. A. Brown, J. Electrochem. Soc. **146**, 2300 (1999).
[3] N. E. B. Cowern, G. Mannino, P. A. Stolk, F. Roozeboom, H. G. A. Huizing, J. G. M. van Berkum, F. Cristiano, A. Claverie, and M. Jaraíz, Phys. Rev. Lett. **82**, 4460 (1999).
[4] G. A. Rozgonyi, A. Karoui, A. Kvit, and G. Duscher, Microelectron. Eng. **66**, 305 (2003).
[5] V. Vaithyanathan, C. Wolverton, and L. Q. Chen, Acta Mater. **52**, 2973 (2004).
[6] T. Sinno, E. Dornberger, R. A. Brown, W. von Ammon, and F. Dupret, Mater. Sci. Eng., R. **R28**, 149 (2000).
[7] M. Prasad and T. Sinno, Appl. Phys. Lett. **80**, 1951 (2002).
[8] N. Cuendet, T. Halicioglu, and W. A. Tiller, Appl. Phys. Lett. **69**, 4071 (1996).
[9] A. Bongiorno, L. Colombo, and T. Diaz De la Rubia, Europhys. Lett. **43**, 695 (1998).
[10] A. Bongiorno, L. Colombo, F. Cargnoni, C. Gatti, and M. Rosati, Europhys. Lett. **50**, 608 (2000).
[11] S. K. Estreicher, J. L. Hastings, and P. A. Fedders, Appl. Phys. Lett. **70**, 432 (1997).
[12] J. Kim, F. Kirchhoff, J. W. Wilkins, and F. S. Khan, Phys. Rev. Lett. **84**, 503 (2000).
[13] M. Goldstein, J. Chem. Phys. **51**, 3728 (1969).
[14] F. H. Stillinger, Science **267**, 1935 (1995).
[15] M. Z. Bazant, E. Kaxiras, and J. F. Justo, Phys. Rev. B **56**, 8542 (1997).
[16] J. F. Justo, M. Z. Bazant, E. Kaxiras, V. V. Bulatov, and S. Yip, Phys. Rev. B **58**, 2539 (1998).
[17] M. Prasad and T. Sinno, Phys. Rev. B **68**, 045207 (2003).
[18] M. Prasad and T. Sinno, Phys. Rev. B **68**, 045206 (2003).
[19] W. G. Hoover, A. C. Hindmarsh, and B. L. Holian, J. Chem. Phys. **57**, 1980 (1972).
[20] D. Frenkel and A. J. C. Ladd, J. Chem. Phys. **81**, 3188 (1984).
[21] D. Frenkel, Phys. Rev. Lett. **56**, 858 (1986).
[22] D. S. Franzblau, Phys. Rev. B **44**, 4925 (1991).
[23] M. Itsumi, H. Akiya, T. Ueki, M. Tomita, and M. Yamawaki, Jpn. J. Appl. Phys., Part 1 **35**, 812 (1996).
[24] F. H. Stillinger and T. A. Weber, Phys. Rev. A **25**, 978 (1982).
[25] S. Sastry, Nature (London) **409**, 164 (2001).
[26] F. Sciortino, W. Kob, and P. Tartaglia, Phys. Rev. Lett. **83**, 3214 (1999).
[27] F. Wang and D. P. Landau, Phys. Rev. Lett. **86**, 2050 (2001).
[28] F. H. Stillinger, J. Chem. Phys. **38**, 1486 (1963).
[29] J. C. Gilbert and J. Nocedal, SIAM J. Control Optim. **2**, 21 (1992).
[30] A. Seeger and K. P. Chik, Phys. Status Solidi **29**, 455 (1968).
[31] D. A. Richie, J. Kim, S. A. Barr, K. R. A. Hazzard, R. Hennig, and J. W. Wilkins, Phys. Rev. Lett. **92**, 045501 (2004).
[32] M. Cogoni, B. P. Uberuaga, A. F. Voter, and L. Colombo, Phys. Rev. B **71**, 121203(R) (2005).
[33] M. P. Allen and D. J. Tildesley, *Computer Simulation of Liquids* (Oxford University Press, Oxford, 1987).
[34] M. T. Zawadzki, W. Luo, and P. Clancy, Phys. Rev. B **63**, 205205 (2001).
[35] The value of α increases by about 10% if regular octahedral geometry is assumed.
[36] K. Nakamura, T. Saishoji, T. Kubota, T. Iida, Y. Shimanuki, T. Kotooka, and J. Tomioka, J. Cryst. Growth **180**, 61 (1997).
[37] R. J. Jaccodine, J. Electrochem. Soc. **110**, 524 (1963).
[38] J. J. Gilman, J. Appl. Phys. **31**, 2208 (1960).
[39] N. Cuendet, T. Halicioglu, and W. A. Tiller, Appl. Phys. Lett. **67**, 1063 (1995).
[40] M. Itsumi, H. Akiya, T. Ueki, M. Tomita, and M. Yamawaki, Jpn. J. Appl. Phys., Part 1 **35**, 812 (1996).
[41] V. V. Voronkov and R. Falster, J. Cryst. Growth **194**, 76 (1998).
[42] T. A. Frewen, S. S. Kapur, W. Haeckl, W. von Ammon, and T. Sinno, J. Cryst. Growth **279**, 258 (2005).
[43] F. Cargnoni, C. Gatti, and L. Colombo, Phys. Rev. B **57**, 170 (1998).
[44] S. Goedecker, T. Deutsch, and L. Billard, Phys. Rev. Lett. **88**, 235501 (2002).
[45] J. Tersoff, Phys. Rev. B **37**, 6991 (1988).
[46] J. Tersoff, Phys. Rev. B **39**, 5566 (1989).